Magnetization-Switched Metal-Insulator Transition in a (Ga,Mn)As Tunnel Device

K. Pappert, M. J. Schmidt, S. Hümpfner, C. Rüster, G. M. Schott, K. Brunner, C. Gould, G. Schmidt, and L. W. Molenkamp
Physikalisches Institut (EP3), Universität Würzburg, Am Hubland, D-97074 Würzburg, Germany
(Received 14 July 2006; published 1 November 2006)

We observe the occurrence of an Efros-Shklovskii gap in (Ga,Mn)As based tunnel junctions. The occurrence of the gap is controlled by the extent of the hole wave function on the Mn acceptor atoms. Using $\mathbf{k}\cdot\mathbf{p}$-type calculations we show that this extent depends crucially on the direction of the magnetization in the (Ga,Mn)As (which has two almost equivalent easy axes). This implies one can reversibly tune the system into the insulating or metallic state by changing the magnetization.

DOI: 10.1103/PhysRevLett.97.186402 PACS numbers: 71.30.+h, 75.30.Hx, 75.50.Pp

A very direct way to observe the Efros-Shklovskii (ES) gap, the soft gap induced by Coulomb correlations near the Fermi level of a Mott insulator [1,2], is by means of tunnel spectroscopy. Such experiments were, e.g., performed on the (three-dimensional) nonmetallic doped semiconductor Si:B [3,4] and on thin (two-dimensional) Be films [5]. While both of these experiments employed large area tunnel junctions and a metallic counter electrode, a more recent study employed Ge:As break junctions [6]. This latter approach avoids possible screening of the Coulomb correlations, but the mesoscopic contacts may complicate extraction of bulk Coulomb gap behavior [7].

We have recently investigated the physics of a novel type of magnetoresistance, dubbed TAMR (tunneling anisotropic magnetoresistance) [8,9]. TAMR results from the dependence of the density of states (DOS) in strongly spin-orbit coupled ferromagnetic semiconductors, such as (Ga,Mn)As, on the direction of the magnetization of the material. In [9] we reported a drastic ($>10^4$) increase of the spin-valve signal in a (Ga, Mn)As/GaAs/(Ga, Mn)As tunnel structure on lowering the sample temperature from 4.2 to 1.7 K, and speculated that this behavior might result from the opening of an ES gap. Here, we provide evidence that the high resistance state of the sample indeed corresponds to a soft-gapped Mott insulator. In these samples, the metal-to-insulator transition (MIT) is driven by a large variation of the Bohr radius of a hole bound to a Mn-impurity when the magnetization of the layer is switched from one easy axis to the other. This assignment is supported by a $\mathbf{k}\cdot\mathbf{p}$-type calculation of a hydrogenlike impurity in a ferromagnetic GaAs host, extending the successful mean-field model for (Ga,Mn)As [10,11].

Our (Ga,Mn)As tunnel structure is shown in Fig. 1(b). From bottom to top, the $Ga_{0.94}Mn_{0.06}As$(100 nm)/GaAs(2 nm)/$Ga_{0.94}Mn_{0.06}As$(10 nm) trilayer stack has been grown by low temperature molecular beam epitaxy (LT-MBE) on a semi-insulating GaAs substrate and a 120 nm undoped GaAs buffer layer. Both (Ga,Mn)As layers are ferromagnetic with an as-grown Curie temperature of ~65 K and highly p-type due to the intrinsic doping arising from the Mn atoms.

As seen in the optical micrograph of Fig. 1(a), the layer stack is patterned into a square mesa of $100 \times 100\ \mu m^2$ by positive optical lithography, metal evaporation, lift-off and wet etching. The top contact is *in situ* Ti/Au. Contact to the lower (Ga,Mn)As layer is established by a W/Au ring around the mesa, fabricated by metal deposition and optical lithography [9].

The structure is intended for vertical tunneling transport experiments. A key element in this device design is that the LT-GaAs tunnel barrier contains many defects, and thus acts as an effective carrier sink, resulting in a thin depleted (Ga,Mn)As region near the barrier and thus band bending near the interfaces, as sketched in Fig. 1(c).

We measure the resistance of the device depending on its magnetic history. Using a magnetocryostat equipped with three pairs of Helmholtz coils, we magnetize the sample along a specific angle φ in the sample plane. One of the magnetic easy axes of the (Ga,Mn)As layers, defined as $\varphi = 0°$, is along the [100] crystal direction. The second, perpendicular, easy axis is along [010] corresponding to

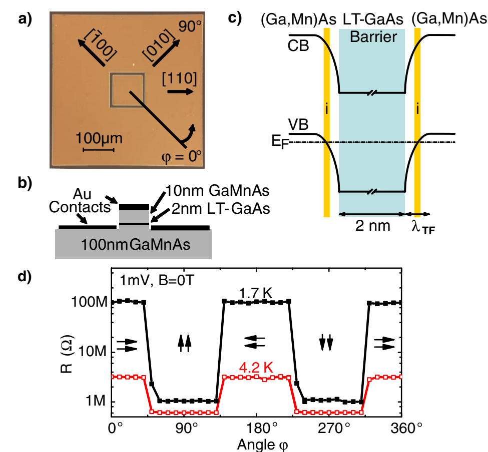

FIG. 1 (color online). (a) Optical micrograph of the sample. (b) Sample layer structure. (c) Schematic band diagram illustrating the barrier for hole transport, the depletion region near the interfaces, and the effective injector layers (i). (d) 4.2 and 1.7 K magnetoresistance in zero field at 1 mV bias after preparing the sample by magnetizing in various field directions φ.

 © 2006 The American Physical Society

$\varphi = 90°$. As the field is swept to zero, the magnetization relaxes to the nearest easy axis, and this magnetization state determines the resistance. Figure 1(d) illustrates the results of such measurement [12] for many preparation angles φ. The 4.2 K-curve can be understood as resulting from TAMR [8]: the anisotropy in the momentum dependent DOS with respect to magnetization direction ([100] or [010]) causes a resistance difference between these two magnetization orientations.

While TAMR is a band structure effect, the extreme amplification of the effect between 4.2 and 1.7 K can only be understood by considering many-particle effects. The data of Fig. 2(a) and 2(b) further support the presence of electron-electron correlations. The differential conductance $G(V) = dI/dV$ in Fig. 2(b) is calculated from current-voltage-characteristics taken in the remanent magnetization state after preparation of the sample at an angle φ. In Fig. 2(a), the $G(V)$ curves at 1.7 K are segregated into two groups associated with each of the two resistance states identified in Fig. 1(d). The magnetization of both (Ga,Mn)As layers relaxes into the low resistance state corresponding to magnetization along [010] for all preparation angles between 45° and 135° [upper curves in Fig. 2(a)]. It relaxes along the [100]-high-resistance state for preparation fields within 45° of the [100] direction (lower curves).

The $G(V)$ characteristics have a distinct shape for each magnetization direction. High conductance curves are square-root-like and show nonvanishing conductance at zero voltage. This is typical for the metallic behavior of doped semiconductors [here (Ga,Mn)As] taking part in the tunnel process. The square root dependence stems from weak localization in metals [13]. The high resistance state, however, shows insulating behavior. The conductance vanishes at zero voltage and the curves follow a higher power law as seen in the log-log plot of Fig. 2(b).

The shape of these $G(V)$ curves is reminiscent of those observed by Lee *et al.* [4] in their investigations of tunneling from a metal into disordered boron-doped silicon near the MIT. Their theory describes the formation of a soft ES gap [1] stemming from an increase in electron-electron Coulomb interaction as screening is reduced when the MIT is approached from the metallic side. This gap around the Fermi energy is observable in the low bias tunneling conductance. It manifests itself in a different power law behavior $G(V) \propto V^m$, with $m = 1/2$ for metallic (just above the MIT) and $m > 2$ for insulating (below the MIT) material.

The transition from metallic to insulating behavior is thermally activated as demonstrated by the zero bias differential resistance data taken at an angle corresponding to the high resistance state at 1.7 K, shown in Fig. 2(c). The data are consistent with an exponential activation following $R \propto \exp(1/T)^{1/2}$ expected for an ES gap material under the usual assumption of single hop tunneling [1,6]. We note, however, that with an accessible temperature range of less than one decade, we cannot rule out an $R \propto \exp(1/T)^{1/4}$ dependence expected from a noncorrelated Mott transition.

A further clue to the origin of our effect comes from the data of Fig. 3 showing the resistance behavior of the sample at 300 mT, a field sufficient to force the magnetization vectors parallel to the field direction for all field angles. The figure shows very strong and apparently random oscillations reminiscent of quantum interference effects, and likely arising from a statistically defined electronic state in the sample. Figure 3(a)–3(c) show that the amplitude of these oscillations grows significantly with reduced bias for angular ranges (gray regions in the figure) associated with ES behavior. Figure 3(c)–3(e) show a significant effect upon thermal cycling to temperatures of some tens of K (above the ES activation temperature). The three curves are nominally identical measurements after

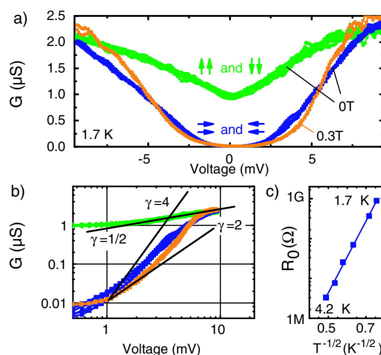

FIG. 2 (color online). (a) Differential conductance-voltage curves at 1.7 K including sets of curves belonging to the two magnetization states at $B = 0$, and one set at $B = 300$ mT along $\varphi = 3°$ and 6°. (b) Log-log plot of the same data. (c) Temperature dependence of the zero bias resistance of the high resistance state.

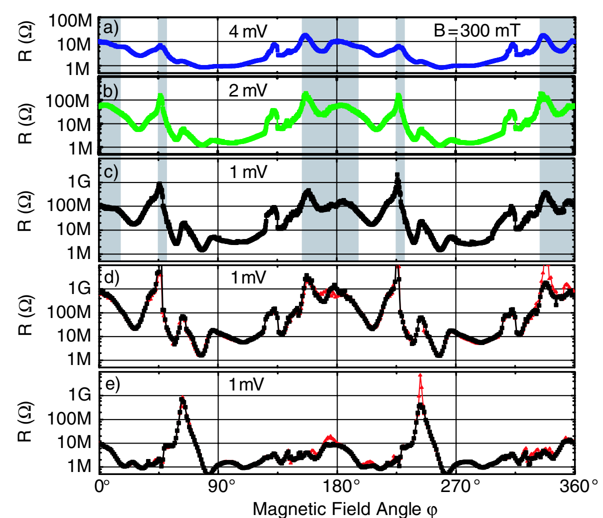

FIG. 3 (color online). Resistance of the sample at 1.7 K and 300 mT as a function of magnetic field direction under various bias and on different cooldowns. (d) and (e) each show the results of two separate measurement, confirming reproducibility.

subsequent thermal cycling. The main behavior of the device remains unchanged, but the details of the fluctuations change significantly, presumably corresponding to a new impurity configuration. We emphasize that the change in the fluctuation pattern is due to thermal cycling. On a given cooldown, measurements are reproducible as confirmed by the two, almost indistinguishable, sets of measurements included in each of Fig. 3(d) and 3(e). $G(V)$ curves at 300 mT along the $\varphi = 3$ and 6° given in Fig. 2(c) show behavior similar to the other high resistance curves.

We attribute these fluctuations to quantum interference effects on the variable range hopping that is the transport mechanism in the insulating state [14]. In Ref. [15], such quantum interference was confirmed by a statistical analysis of the amplitude of the fluctuations as the Fermi energy is varied using an external gate bias. A similar analysis cannot be reliably applied here as the relation between the magnetization direction and the Fermi energy is complex and nonlinear.

The behavior of our sample is fully consistent with the depleted (Ga,Mn)As injection layer undergoing a MIT triggered by a reorientation of the magnetization from [010] to [100], and the formation of an ES-gap. In order to understand how a change in magnetization direction can trigger a MIT, we need to consider the criterion for the passage from metallic to insulating properties.

Metallic transport properties require the charge carriers to be in long range itinerant states. This condition implies significant overlap of the wave functions between acceptors (Mn atoms). As such, the passage through the MIT depends not only on the carrier density, but also on the volume occupied by the wave functions of the states of the individual dopants. Indeed a change in impurity conductivity associated with a strain induced change in Bohr radius has been reported previously [16].

For (Ga,Mn)As, it is well established [10,11] that details of the DOS are influenced by the magnetization direction. To determine if this plays a role in renormalizing the wave function extent of our localized states, we turn to a numerical calculation of bound hole states.

The valence band in a zinc blende semiconductor is described in a 6-band $\mathbf{k}\cdot\mathbf{p}$ framework by the full Luttinger Hamiltonian $H(\mathbf{k})$ [17]. Luttinger and Kohn showed [18] that a charged impurity in a semiconductor host can be described by treating the impurity wave function as an envelope wave function $\mathbf{B}(\mathbf{k})$ of Bloch waves. The time-independent Schrödinger equation is then [18]:

$$H(\mathbf{k})\mathbf{B}(\mathbf{k}) + \int d^3\mathbf{k}'\,\mathcal{U}(\mathbf{k}-\mathbf{k}')\mathbf{B}(\mathbf{k}') = E_b\mathbf{B}(\mathbf{k}), \quad (1)$$

where E_b is the binding energy. $\mathcal{U}$ is the Fourier transform of the Yukawa potential between the hole and the impurity center. $H(\mathbf{k})$ is a 6×6 matrix acting on the six-dimensional vector $\mathbf{B}(\mathbf{k})$ locally in $\mathbf{k}$ space. It describes the band structure including, for magnetic (Ga,Mn)As, pd exchange, strain, and SO coupling. Equation (1) is solved numerically, in the limit of an unscreened Coulomb potential, for the acceptor ground state in a magnetic zinc blende semiconductor. The obtained k-space wave functions are fitted to hydrogen ground state wave functions in order to extract an effective Bohr radius for each k direction and for various magnetization directions. Details of these calculations will be published elsewhere.

From symmetry considerations, one expects that our (Ga,Mn)As has fourfold in-plane magnetic easy axes. Experimentally however, a ~100-fold weaker [010] uniaxial anisotropy is generally observed in samples from various sources. While the origin of this uniaxial anisotropy is unknown, considerable insight is gained by phenomenologically introducing a uniaxial strain term ϵ_u along [010] [8]. An important result of the bulk band structure calculation is that the energy ordering of the bands depends on the relative strain and magnetization directions. In Fig. 4(a), the Γ point energy of the top 4 valance bands is plotted as a function of the amplitude of ϵ_u and the pd exchange. For zero strain, we obtain the expected [10,11] nearly equidistant spacing between the 4 bands, while increasing strain shifts the relative energy position of the light-hole-like bands with respect to the heavy-hole-like bands, leading to a change in ordering of the bands at the line defining the crossing point between the top two planes in the figure, and thus to a profound change in the character of the wave function at a given energy. This is directly reflected in the wave function of the impurity hole state.

Figure 4(b) shows the extent of a bound hole for magnetization along different in-plane easy axes with an amplitude of ϵ_u beyond the crossing point for the bulk energy at the Γ-point. There is a significant difference in the size of the wave function between the $\vec{M} \parallel \epsilon_u$ and the $\vec{M} \perp \epsilon_u$-state. The result is that the wave function overlap be-

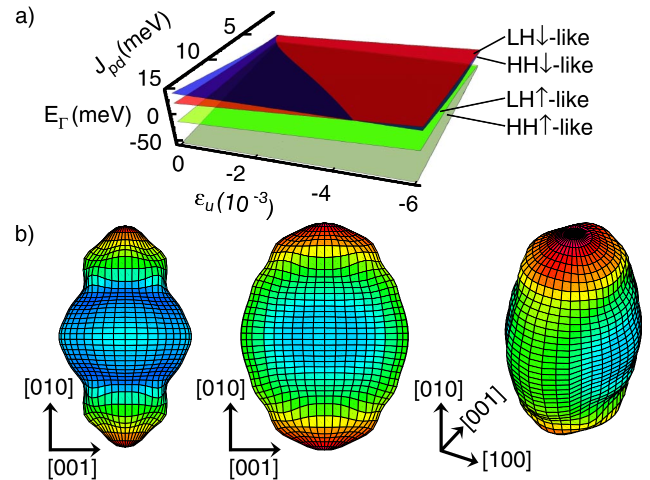

FIG. 4 (color online). (a) Γ point energy of the four top bands as a function of strain ϵ_u and pd exchange. The top layers meet at the origin of all 3 axes in the upper left corner. For reference, the growth strain in the layer is $\epsilon \sim 0.004$ (b) Extents of a hole bound to a Mn-impurity. [001] is the growth direction and ϵ_u is along [010]. Left: Magnetization $\mathbf{M} \parallel$ [100]. Middle: $\mathbf{M} \parallel$ [010]. Right: Perspective view for $\mathbf{M} \parallel$ [010].

tween neighboring dopant sites depends on the direction of the magnetization, and for reasonable parameters is consistent with the observation of the magnetization reorientation induced MIT.

It is important to note that the above calculation does not predict a MIT for the bulk (Ga,Mn)As which, as typical in high quality (Ga,Mn)As, has nearly temperature independent resistivity in the temperature range of interest. Our prediction is limited to the thin (Ga,Mn)As layer near the interface with the tunnel barrier. The barrier consists of LT-GaAs, a material with many midgap traps and leading to a gradual spatial depletion of the (Ga,Mn)As near the barrier on the length scale of the Thomas-Fermi screening length of $\sim$2 Å, and thus to a much lower effective local carrier density, as illustrated schematically in Fig. 1(c). If the thin depleted layer is close enough to the MIT, a change in the wave function extent can trigger the transition. Another point is that the mean-field *pd* exchange strength is smaller for lower hole densities. As seen in Fig. 4, a weaker *pd* exchange lowers the amplitude of ϵ_u needed to reach the band crossing to values that are consistent with those used in the original description of TAMR [8,9].

A key point here is that while this thin depleted layer plays a limited role in the magnetic properties, because the mean free path of holes in (Ga,Mn)As is of the order of a few Å, it still has a dominant effect on the transport. Combining the fact that, by definition, the transition from diffusive to tunneling transport takes place at a density where holes can no longer classically diffuse, with this extremely short mean free path, must lead to a very thin effective injector layer from which the tunneling originates. This injection layer is characterized by considerably reduced carrier density relative to the bulk, and thus consistent with our model description above.

The link between the MIT and the development of an ES gap is that the reduction in mobile carriers reduces screening. With unscreened Coulomb interactions between localized states, the DOS at the Fermi energy for carrier concentrations just below the MIT vanishes with a dimension-dependent power law [1], i.e., $D(\epsilon) \propto \epsilon$, where ϵ is the energy measured with respect to the Fermi energy, for two-dimensional materials, and $D(\epsilon) \propto \epsilon^2$ in three dimensions. Of course, we cannot rule out that the change in screening causes a slight shift in position of the effective injector thus modifying the tunneling distance, and accounting for part of the observed resistance change.

Larkin and Shklovskii [7] derived a power law behavior for conductance versus voltage (G-V) curves for tunneling between two three-dimensional localized materials where the parabolic DOS $D(\epsilon) \propto \epsilon^2$ on each side multiply and lead to $G \propto V^6$. In our case, given the very thin nature of the injector, a 2D description of the DOS of the tunneling reservoirs is likely more appropriate. Thus, the DOS is linear in energy, and the expected power of the G-V curves is 4. Moreover, it is unclear in our experiment whether both sides of the barrier play an equivalent role, or whether the effects are dominated by one electrode. Depending on the relative role of the two barriers, one would thus expect a power law somewhere between $\propto V^2$ and $\propto V^6$. Neglecting very low voltages where thermal smearing is important, this prediction is in good agreement with the experimental observation of Fig. 2.

In conclusion, we have observed the magnetization reorientation induced MIT in a (Ga,Mn)As based transport sample. The transition can be understood as stemming from a modification of the wave functions of individual dopants due to the coupling of the Mn dopants to the magnetization direction in the bulk. Furthermore, the transition is accompanied by the opening of an ES gap at the Fermi energy which manifests itself as a change in the power law behavior in conductance-voltage characteristics in tunneling experiments. This is the first observation of a MIT induced by a change in magnetization *direction* in any material. In addition to the fundamental interest intrinsic to these observations, the results may also have technological relevance in opening up new possibilities of controlling the transport properties of devices by magnetization reversal.

The authors thank R. Opperman, M. Flatté, R. Giraud, and B. I. Shklovskii for useful discussions and V. Hock for sample preparation. We acknowledge financial support from the EU (SPINOSA and No. FP6-IST-015728, NANOSPIN), the German BMBF (No. 13N8284) and DFG (No. BR1960/2-2).

[1] A. L. Efros and B. I. Shklovskii, J. Phys. C **8**, L49 (1975).
[2] B. I. Shklovskii and A. L. Efros, *Electronic Properties of Doped Semiconductors* (Springer, New York, 1984).
[3] J. G. Massey and M. Lee, Phys. Rev. Lett. **75**, 4266 (1995).
[4] M. Lee, J. G. Massey, V. L. Nguyen, and B. I. Shklovskii, Phys. Rev. B **60**, 1582 (1999).
[5] V. Yu. Butko, J. F. diTusa, and P. W. Adams, Phys. Rev. Lett. **84**, 1543 (2000).
[6] B. Sandow *et al.*, Phys. Rev. Lett. **86**, 1845 (2001).
[7] A. I. Larkin and B. I. Shklovskii, Phys. Status Solidi B **230**, 189 (2002).
[8] C. Gould *et al.*, Phys. Rev. Lett. **93**, 117203 (2004).
[9] C. Rüster *et al.*, Phys. Rev. Lett. **94**, 027203 (2005).
[10] M. Abolfath, T. Jungwirth, J. Brum, and A. H. MacDonald, Phys. Rev. B **63**, 054418 (2001).
[11] T. Dietl, H. Ohno, and F. Matsukura, Phys. Rev. B **63**, 195205 (2001).
[12] Because the current in the high resistance state is comparable to amplifier offsets, offset correction casts doubts on the accuracy of values above 1 GΩ.
[13] B. L. Altshuler and A. G. Aronov, Sov. Phys. JETP **50**, 968 (1979).
[14] V. L. Nguen, B. Z. Spivak, and B. I. Shklovskii, Sov. Phys. JETP **62**, 1021 (1985); M. E. Raikh and I. M. Ruzin, Sov. Phys. JETP **65**, 1273 (1987).
[15] R. J. F. Hughes *et al.*, Phys. Rev. B **54**, 2091 (1996).
[16] F. H. Pollak, Phys. Rev. **138**, A618 (1965).
[17] T. Dietl, H. Ohno, and F. Matsukura, Phys. Rev. B **63**, 195205, (2001).
[18] J. M. Luttinger and W. Kohn, Phys. Rev. **97**, 869 (1955).